# Development of the Ca−Au−In Icosahedral Quasicrystal and Two Crystalline Approximants: Practice via Pseudogap Electronic Tuning

Qisheng Lin and John D. Corbett*

*Contribution from the Department of Chemistry, Iowa State University, Ames, Iowa 50010*

Received December 20, 2006; E-mail: jcorbett@iastate.edu

**Abstract:** Electronic tuning and syntheses to gain the icosahedral quasicrystal (i-QC) ($Ca_{14.1(2)}Au_{44.2(8)}In_{41.7(7)}$, e/a = 1.98) and two approximant crystals (ACs) are reported. The tuning was derived from $Na_2Au_6In_5$, another cubic $Mg_2Zn_{11}$-type structure, for which the Fermi level (e/a = 1.77) should tune to a calculated pseudogap (e/a = 2.02) under a rigid band assumption. The 1/1 AC, $Ca_3Au_{12.2(1)}In_{6.3(2)}$ (e/a = 1.73), crystallizes in space group $Im\bar{3}$, with a = 15.152(2) Å, Z = 8, and the 2/1 AC, $Ca_{12.6(1)}Au_{37.0(2)}In_{39.6(6)}$ (e/a = 2.01), in $Pa\bar{3}$, with a = 24.632(3) Å , Z = 8. Both have substantially fixed compositions according to lattice dimensions. Structure analyses reveal that both ACs contain triacontahedral clusters as the basic building blocks at the body-centered and primitive cubic unit cell levels, respectively. Densities-of-states (DOS) analyses for the 1/1 AC structure reveal a pseudogap at e/a = 2.00, close to the point at which the i-QC was predicted and experimentally tuned. Phase relationships of the ACs and the i-QC are reported according to DTA, XRD, and temperature-dependent XRD measurements. The QC is thermodynamically metastable below ~500 °C.

## Introduction

Quasicrystals (QCs) are a class of intermetallic compounds featuring forbidden rotational (5-, 8-, 12-fold, etc.) symmetries,[1−3] and their structures in turn result in atypical properties, such as low surface energy, low friction coefficient, high tensile strength, and low thermal conductivity. These unique characteristics suggest prospective and potential QC applications in alloys, surface coatings, power generation/cooling, hydrogen storage, biomaterials, and catalysis.[4−7] In contrast to the advances in material applications, the strategies for developing novel QC systems and the knowledge of QC structures are still far from complete. Therefore, exploratory syntheses of new approximant crystals (ACs) and their transformation to respective QCs are important since ACs have been assumed to contain the same local building blocks as QCs and to have similarly close chemical compositions.[8]

As we know, ~75% elements in the Periodic Table are metals, and the possible combinations of metallic elements must afford a very large number of binary, ternary, and quaternary intermetallic compounds. Among these are the presumably very select group that exhibits quasicrystalline phenomena. In principle, valence electron counts (VEC) or electrons per atom

(e/a) values are believed to be very important empirical factors in determining the stabilities and complex structure−property relationships of many compounds. For example, the Hume−Rothery rules[9] yield a unique interpretation of particularly stable intermetallic compounds in terms of similar-sized Femi spheres and Brillouin zone boundaries, whereas the Wade−Mingos rules[10,11] successfully relate the geometries of stable deltahedral clusters to the number of skeletal electron pairs in certain Zintl phases or clusters. Not surprisingly, QCs, which are also thought to be special intermetallics, appear to have close relationships to certain e/a values. Actually, e/a values for decagonal (2D) QCs appear to converge at 1.75, whereas those of icosahedral QCs (i-QCs) usually fall in the range of 2.0−2.2.[12] These values suggest that QCs may be electronically positioned between the Hume−Rothery (<2.0) and the classical Zintl phases (≥4.0).

Guided by the fact that the Fermi levels of QCs evidently fall in electronic pseudogaps,[13,14] an electronic tuning route by which the Fermi level ($E_F$) of a selected intermetallic is displaced to the center of calculated pseudogap has been developed[15] and successfully applied in the Sc−Mg−Cu−Ga[15,16] and Sc−Mg−Zn systems.[17] The evolution of both started with particular intermetallics with $Mg_2Zn_{11}$-type structures, $Mg_2Cu_6Ga_5$ and $Mg_2Zn_{11}$, respectively, which contain components from both

(1) Janot, C. *Quasicrystals: A Primer*, 2nd ed.; Oxford University Press: Oxford, UK, 1994.
(2) Lifshitz, R. *Found. Phys.* **2003**, *33*, 1703.
(3) Shechtman, D.; Blech, I.; Gratias, D.; Cahn, J. W. *Phys. Rev. Lett.* **1984**, *53*, 1951.
(4) Kelton, K. F.; Gibbons, P. C. *MRS Bull.* **1997**, *71*.
(5) Andersen, B. C.; Bloom, P. D.; Baikerikar, K. G.; Sheares, V. V.; Mallapragada, S. K. *Biomaterials* **2002**, *23*, 1761.
(6) Kameoka, S.; Tanabe, T.; Tsai, A. P. *Catal. Today* **2004**, *93−95*, 23.
(7) Macia, E. *Appl. Phys. Lett.* **2000**, *77*, 3045.
(8) Goldman, A. I.; Kelton, K. F. *Rev. Mod. Phys.* **1993**, *65*, 213.

(9) Hume-Rothery, W. *J. Inst. Met.* **1926**, *35*, 295.
(10) Wade, K. *Adv. Inorg. Chem. Radiochem.* **1976**, *18*, 1.
(11) Mingos, D. M. P. *J. Chem. Soc., Chem. Commun.* **1983**, 706.
(12) Tsai, A. P. In *Physical Properties of Quasicrystals*; Stadnik, Z. M., Ed.; Springer: New York, 1999; pp 5−50.
(13) Pierce, F. S.; Poon, S. J.; Biggs, B. D. *Phys. Rev. Lett.* **1993**, *70*, 3919.
(14) Smith, A. P.; Ashcroft, N. W. *Phys. Rev. Lett.* **1987**, *59*, 1365.
(15) Lin, Q.; Corbett, J. D. *J. Am. Chem. Soc.* **2005**, *127*, 12786.
(16) Lin, Q.; Corbett, J. D. *Inorg. Chem.* **2003**, *42*, 8762.
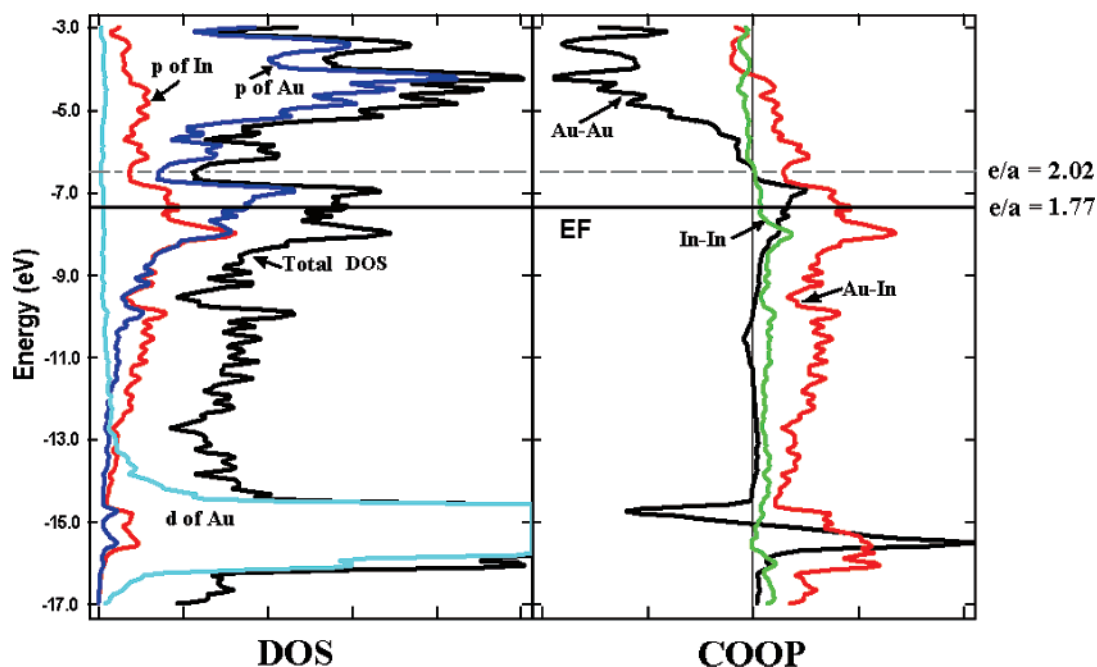(17) Lin, Q.; Corbett, J. D. *Philos. Mag.* **2006**, *86*, 607.

**Figure 1.** Densities-of-states (DOS) and crystal orbital overlap population (COOP) data for $Na_2Au_6In_5$ showing the pseudogap (e/a = ~2.02) and empty bonding states above $E_F$ (e/a = 1.77).

the Hume−Rothery phase region (i.e., Cu, Zn) and the region of the Zintl border (i.e., Ga). Moreover, both compounds exhibit multi-endohedral clusters with local pseudo 5-fold symmetries and have apparent pseudogaps and empty bonding states somewhat above $E_F$.[16] Appropriate chemical substitutions to drive $E_F$ to the pseudogap in a rigid band sense then follow. These successes naturally raised the question as to whether the tuning process starting from $Na_2Au_6In_5$[18] (another member of the small $Mg_2Zn_{11}$ family) to gain a novel i-QC is feasible (Figure 1).

To this end, this work presents in detail the design, again aided by the existence of a pseudogap in this precursor, the exploratory syntheses, the structure and properties determined for the 1/1 AC and 2/1 ACs, and the electron tuning to an i-QC in this new system. The work continues to support the ideas that pseudogap tuning is a useful route to novel QC systems, at least in certain systems, and that quasicrystals are not far away from phases and structures that solid-state chemists have studied before, especially in the field of intermetallic compounds.[19,20]

## Experimental Section

**Syntheses.** Syntheses were performed via reactions of the as-received elements, calcium chunks, granular gold, and indium tear drops (all >99.9%, Alfa). These were weighed in a glovebox filled with nitrogen and welded/sealed under an argon atmosphere into tantalum containers, which were in turn held within evacuated $SiO_2$ jackets to avoid air oxidation. Samples were heated to 800 °C, held at this temperature for 24 h, and then treated under different conditions to yield different products. ACs were obtained after cooling (10 °C/h) and annealing treatments (200−500 °C for 2−30 days), whereas the i-QC was obtained only by quenching. Later on, arc-melting syntheses were also found to result in high yields (>95%) of the i-QC phase.

**Powder X-ray Diffraction.** Data acquisitions were made on a Huber 670 Guinier powder camera equipped with an area detector and Cu

Kα₁ radiation ($\lambda = 1.540598$ Å). Finely powdered samples were homogeneously dispersed on a flat Mylar film with the aid of vacuum grease. The step length was set to 0.005°, and the exposure time was 0.5 h. The detection limit of a second phase is conservatively estimated as about 5 atom % in equivalent scattering power.

**SEM-EDX.** The elemental compositions were determined via semiquantitative energy-dispersive X-ray spectroscopy (EDX) on a JEOL 840A scanning electron microscope (SEM) with IXRF X-ray analyzer system and Kevex Quantum light-element detector. To increase the accuracies, samples mounted in epoxy were carefully polished to avoid the influence of sample tilting. At least four readings were made on each sample, with the averages being compared with the refined compositions from X-ray diffraction data. Electron diffraction was used to identify the i-QC. This was accomplished with the aid of a JEOL 3000 field emission transmission electron microscope (TEM) and 300 kV electrons. The ED pattern of the present i-QC along the 5-fold zone axis is shown below.

**Thermal analyses.** Thermal analyses of 1/1 AC, 2/1 AC and i-QC samples were performed under argon atmosphere on a Perkin-Elmer Differential Thermal Analyzer (DTA-7). Samples were typically heated to 620 °C at a rate of 10 °C/min, kept at this temperature for 10 min, then cooled to 200 °C at the same rate. XRD patterns were recorded before and after each DTA scan.

**Temperature-Dependent Powder X-ray Diffraction.** In order to study the phase transitions of the 2/1 AC and i-QC in situ, the temperature-dependent powder X-ray diffraction analyses were performed on a custom-built Rigaku powder diffractometer (TTRAX III) equipped with Mo Kα radiation and a high-temperature attachment (±3 °C). Fine powders with $\phi < 50 \mu$m were mounted on a platinum sample holder and held in a chamber evacuated to ~3 × $10^{-3}$ Torr. To avoid sample exposure and oxidation as much as possible, data were regularly collected only within the range of 15° ≤ 2θ ≤ 20°, with a scan speed of 0.02° s⁻¹.

**Single-Crystal Structure Determinations.** Data collections were performed with the aid of a Bruker APEX CCD single-crystal diffractometer equipped with graphite-monochromatized Mo Kα ($\lambda = 0.71069$ Å) radiation. The exposure time was 30 s per frame. Data integration, absorption, and Lorentz polarization corrections were done by the SAINT and SADABS subprograms included in the SMART

(18) Zachwieja, U. *J. Alloys Compd.* **1996**, *235*, 7.
(19) Corbett, J. D. *Angew. Chem., Int. Ed.* **2000**, *39*, 670.
(20) Dong, Z.-C.; Corbett, J. D. *Angew. Chem., Int. Ed.* **1996**, *35*, 1006.

software packages.[21] Assignments of the space groups from the diffractometer data were made on the basis of the Laue symmetry and systematic absence analyses. Structure refinements were performed with the aid of the SHELXTL subprogram.[21]

For the 1/1 AC ($Im\bar{3}$), several data sets were collected from different crystals to check compositional variations. Here the refinement of a crystal from the reaction composition $Ca_{13.9}Au_{56.2}In_{29.9}$ is taken as an example. Seven atoms were first located by direct methods; the first six had separations suitable for Au/In atom pairs, and the seventh, for Ca−Au/In. The former were initially assigned to Au, and the latter, to Ca. Subsequent least-square refinements proceeded smoothly and converged at $R_1 \approx 19.4\%$. Examination of the resulting isotropic displacement parameters indicated that five of six atoms assigned as Au were too electron-rich compared with the other ($U_{iso}$: 0.028 vs 0.003 $Å^2$); thus, the former were tentatively assigned to indium in the followed refinements. Rechecking the thermal parameters after a few cycles revealed that four of these last positions had smaller isotropic values (0.009−0.015 $Å^2$) than the average of the other two (0.026 $Å^2$), suggesting that the former were occupied by Au/In mixtures. Accordingly, Au/In admixtures at each of these positions were allowed to vary (with the total occupancies fixed at 100%) along with a single isotropic displacement parameter in subsequent refinements. At this stage, a difference Fourier map revealed two other clear peaks at a 24g (0, 0.068, 0.086) and the 8c (1/4, 1/4, 1/4) sites that had slightly shorter bond distances (2.47−2.67 Å) to their neighbor atoms. The former is located in the center of a dodecahedron (see structure description below) and generates a distorted icosahedron or cubeoctahedron. (This is usually considered to be a disordered tetrahedron in Tsai-type systems with ∼1/3 occupancy,[22,23] whereas the latter resides in a sometimes empty cube.[24]) The isotropic displacement parameters of these two atoms were also 2−3 times the average for the others atoms (0.06 $Å^2$), signatures of partially occupied sites. Even so, it was noteworthy that after least-squares refinements with anisotropic parameters, which converged at $R_1 \approx 7.9\%$, the difference Fourier map still had two large residual peaks, one (∼15.5 e·$Å^{-3}$) about 0.6 Å from the fractional In5/Au5 and the other (14.2 e·$Å^{-3}$), about 1.2 Å from In4/Au4. Close examination of the observed Fourier map (Figure S1) revealed that the latter two atoms had irregularly elongated densities, suggesting that these residuals truly represented split positions. They were so assigned, and the final anisotropic refinements drastically decreased to $R_1 = 4.98\%$, $R_w = 11.36\%$ for 56 variables and 797 independent reflections. The maximum and minimum peaks in the final difference Fourier map were 5.73 and −4.31 e·$Å^{-3}$, respectively. The refined composition is $Ca_3Au_{12.2(1)}In_{6.3(2)}$, or normalized, as $Ca_{14.0}Au_{56.7(5)}In_{29.3(8)}$, well consistent with the EDX result, $Ca_{13.9(5)}Au_{56.2(4)}In_{29.9(5)}$.

As for the 2/1 AC, the refinement of a crystal from a reaction composition of $Ca_{14.0}Au_{41.6}In_{44.4}$ is taken as an example. Direct methods yielded 34 positions; of these, 29 had separations suitable for Au/In atom pairs and five, for Ca−Au/In. They were initially assigned to Au and Ca. Subsequent least-squares refinements in $Pa\bar{3}$ converged quickly to $R_1 \approx 16\%$. However, 17 of the original Au atoms now had isotropic thermal parameters 6−7 times larger than the average of other positions ($U_{iso}$: 0.037 $Å^2$ vs 0.005 $Å^2$), and so these positions were temporary assigned to In. After a few cycles of refinements, the isotropic displacement parameters revealed two kinds of variations: In27, In28, In29, and Ca35 had anomalously large values ($U_{iso}$ = 0.346−0.145 $Å^2$), whereas In4, In10, In13, In14, and In15 positions had thermal parameters too small (∼1 × $10^{-5}$ $Å^2$). These suggested that the first four positions might be partially occupied and the latter five were occupied by Au/In admixtures. They were so assigned in the following refinements, which converged smoothly at $R_1 \approx 8.8\%$. But the difference map at this stage revealed two other possible atoms; one

(21) *SHELXTL*; Bruker AXS, Inc.: Madison, WI, 1997.
(22) Larson, A. C.; Cromer, D. T. *Acta Crystallogr., Sect. B* **1971**, *27*, 1875.
(23) Pay Gómez, C.; Lidin, S. *Phys. Rev. B* **2003**, *68*, 024203.
(24) Piao, S.; Gomez, C. P.; Lidin, S. *Z. Nat.* **2006**, *61*, 644.

**Table 1.** Crystal Data and Structure Refinement for 1/1 and 2/1 ACs

| refined formula | $Ca_3Au_{12.2(1)}In_{6.3(2)}$ | $Ca_{12.6(1)}Au_{37.0(2)}In_{39.6(6)}$ |
|---|---|---|
| formula weight | 3239.2 | 12342.6 |
| space group , Z | $Im\bar{3}$, 8 | $Pa\bar{3}$, 8 |
| latt. para.(Å) | 15.152(2) | 24.603(3) |
| $V$ ($Å^3$)/$d_{cal}$ (g/cm$^3$) | 3478.6(7)/12.37 | 14945.0(3)/10.97 |
| absorption coefficient (mm$^{-1}$) | 111.2 | 85.1 |
| refl. coll./obs. [$I > 2\sigma(I)$]/$R_{int}$ | 10483/670/0.074 | 91239/4105/0.172 |
| data/restraints/parameters | 797/0/56 | 6129/0/300 |
| $R_1/R_w$ [$I > 2\sigma(I)$] | 0.0498/0.1136 | 0.0557/0.1242 |
| $R_1/R_w$ (all data) | 0.0614/0.1180 | 0.0980/0.1432 |
| residual peaks (e·$Å^{-3}$) | 5.73/−4.30 | 5.48/−7.00 |

(∼42.2 e·$Å^{-3}$) about 1.79 Å from In28 and another (∼21.4 e·$Å^{-3}$), about 0.67 Å from In23. The short separations suggested that they were split positions related to In28 and In23, respectively, and the observed Fourier map also showed elongated electron densities encompassing these two pairs of positions (Figure S1). The final anisotropic refinement converged at $R_1 = 5.57\%$, $R_w = 12.42\%$ for 300 variables and 6129 independent reflections. The maximum and minimum peaks in the final difference Fourier map were 5.44 and −7.00 e·$Å^{-3}$. The refined composition was $Ca_{12.6(1)}Au_{37.0(2)}In_{39.6(6)}$ (e/a = 2.03), or normalized as $Ca_{14.1(1)}Au_{41.5(2)}In_{44.4(6)}$, in good agreement with the EDX result, $Ca_{14.4(4)}$-$Au_{42.7(4)}In_{43.2(5)}$. Note that the composition of 2/1 AC is extremely close to that of i-QC, $Ca_{14.1(2)}Au_{44.2(8)}In_{41.7(7)}$ (EDX result, e/a = 1.98), but notably different from that of the 1/1 AC, $Ca_{13.9(5)}Au_{56.2(4)}In_{29.9(5)}$ (EDX, e/a = 1.74).

A summary of crystal and structural refinement data for both crystals is in Table 1, and the refined positional parameters standardized with TIDY[25] are listed in Table 2 together with their isotropic−equivalent displacement ellipsoids. It should be noted that the 2/1 AC characteristically exhibits a large number of relatively weak reflection data, resulting in the generally larger $R_{int}$ and $R_1$ values for all data (Table 1). The remaining data (anisotropic displacement parameters and bond distances) are in Tables S1 and S2 and in deposited CIF data (Supporting Information).

**Electronic Structure Calculations.** The electronic structure of $Na_2Au_6In_5$ was calculated with the aid of CAESAR,[26] according to semiempirical extended-Hückel-tight-binding (EHTB) methods. As usual, Na atoms were assumed to be fully ionized, each providing one electron to the $(Au_6In_5)^{2-}$ anion network, and they were not included in the input. The following orbital energies and exponents were employed in the calculation ($H_{ii}$ = orbital energy (eV), $\xi$ = Slater exponent): Au 6s, $H_{ii}$ = −10.92, $\xi$ = 2.602; 6p, $H_{ii}$ = −5.55, $\xi$ = 2.584; 5d, $H_{ii}$ = −15.076, $\xi_{11}$ = 6.163, c1 = 0.6851; $\xi_{22}$ = 2.794, c2 = 0.5696;[27] In 5s, $H_{ii}$ = −12.6, $\xi$ = 1.903; 5p, $H_{ii}$ = −6.19, $\xi$ = 1.677.[28]

Electronic band structure calculations on the 1/1 AC were performed by the self-consistent, tight-binding, linear-muffin-tin-orbital (LMTO) method[29−31] in the local density (LDA) and atomic sphere (ASA) approximations, within the framework of the DFT method.[32] Interstitial spheres were introduced in order to achieve space filling. The ASA radii as well as the positions and radii of these empty spheres were calculated automatically, and the values so obtained were all reasonable. Reciprocal space integrations were carried out using the tetrahedron

(25) Gelato, L. M.; Parthé, E. *J. Appl. Crystallogr.* **1987**, *20*, 139.
(26) Ren, J.; Liang, W.; Whangbo, M.-H. *CAESAR for Windows*; Prime-Color Software Inc., North Carolina State University: Raleigh, NC, 1998.
(27) Komiya, S.; Albright, T. A.; Hoffmann, R.; Kochi, J. K. *J. Am. Chem. Soc.* **1977**, *99*, 3036.
(28) Hinze, J.; Jaffé, H. H. *J. Phys. Chem.* **1963**, *67*, 1501.
(29) Shriver, H. L. *The LMTO Method*; Springer-Verlag: Berlin, Germany 1984.
(30) Anderson, O. K.; Jepsen, O. *Phys. Rev. Lett.* **1984**, *53*, 2571.
(31) Jepsen, O.; Snob, M. *Linearized Band Structure Methods in Electronic Band-Structure and its Applications, Springer Lecture Note*; Springer-Verlag: Berlin, Germany, 1987.
(32) Tank, R.; Jepsen, O.; Burckhardt, A.; Andersen, O. K. *TB-LMTO-ASA Program,* Vers. 4.7; Max-Planck-Institut für Festkörperforschung: Stuttgart, Germany 1988.

***Table 2.*** Atomic Coordinates and Equivalent Isotropic Displacement Parameters for Ca$_3$Au$_{12.2(1)}$In$_{6.3(2)}$ 1/1 AC and Ca$_{12.6(1)}$Au$_{37.0(2)}$ In$_{39.6(6)}$ 2/1 AC

| | Wyck. | occupancy | *x* | *y* | *z* | *U*(eq)$^a$ (Å$^2$) |
|---|---|---|---|---|---|---|
| | | | 1/1 AC | | | |
| Au1 | 24g | 1 | 0 | 0.4042(1) | 0.3470(1) | 0.022(1) |
| Au/In2 | 48h | 0.75/0.25(1) | 0.1091(1) | 0.3415 (1) | 0.1994(1) | 0.035(1) |
| In3 | 12e | 1 | 0 | 1/2 | 0.1900(2) | 0.023(1) |
| In4 | 16f | 0.148 (8) | 0.1087(9) | *x* | *x* | 0.033(1) |
| Au4 | 16f | 0.852(8) | 0.1560(1) | *x* | *x* | 0.033(1) |
| In5 | 24g | 0.29(1) | 0 | 0.2111(1) | 0.0866(6) | 0.026(1) |
| Au5 | 24g | 0.71(1) | 0 | 0.2487(3) | 0.0911(1) | 0.026(1) |
| In/Au6 | 12d | 0.45/0.55(2) | 0 | 0.5924(1) | 0 | 0.031(1) |
| In7 | 24g | 0.33(1) | 0 | 0.0676(6) | 0.0848(6) | 0.056(3) |
| In8 | 8c | 0.47(2) | 1/4 | 1/4 | 1/4 | 0.066(5) |
| Ca | 24g | 1 | 0.1962(4) | 1/2 | 0.3128(4) | 0.028(1) |
| | | | 2/1 AC | | | |
| Au1 | 24d | 1 | 0.4038(1) | 0.3448(1) | 0.016(1) | |
| Au2 | 24d | 1 | 0.0557(1) | 0.3995(1) | 0.3459(1) | 0.017(1) |
| Au3 | 24d | 1 | 0.3456(1) | 0.4453(1) | 0.4086(1) | 0.019(1) |
| Au/In4 | 24d | 0.81/0.19(1) | 0.1547(1) | 0.3515(1) | 0.3974(1) | 0.015(1) |
| Au5 | 24d | 1 | 0.0959(1) | 0.4620(1) | 0.2492(1) | 0.019(1) |
| Au6 | 24d | 1 | 0.0570(1) | 0.2484(1) | 0.2488(1) | 0.014(1) |
| Au7 | 8c | 1 | 0.2496(1) | *x* | *x* | 0.013(1) |
| Au8 | 24d | 1 | 0.0928(1) | 0.3107(1) | 0.1510(1) | 0.014(1) |
| Au9 | 24d | 1 | 0.0755(1) | 0.2177(1) | 0.4489(1) | 0.013(1) |
| Au/In10 | 24d | 0.76/0.24(1) | 0.2143(1) | 0.4491(1) | 0.2418(1) | 0.014(1) |
| Au11 | 24d | 1 | 0.0678(1) | 0.0953(1) | 0.4676(1) | 0.015(1) |
| Au/In12 | 24d | 0.38/0.62(1) | 0.0568(1) | 0.0576(1) | 0.2524(1) | 0.018(1) |
| Au/In13 | 24d | 0.69/0.31(1) | 0.0005(1) | 0.1540(1) | 0.0980(1) | 0.018(1) |
| Au/In14 | 24d | 0.66/0.34(1) | 0.2301(1) | 0.4705(1) | 0.4493(1) | 0.023(1) |
| Au/In15 | 24d | 0.42/0.58(1) | 0.0806(1) | 0.4700(1) | 0.4415(1) | 0.025(1) |
| In16 | 8c | 1 | 0.3488(1) | *x* | *x* | 0.011(1) |
| In/Au17 | 24d | 0.72/0.28(1) | 0.0978(1) | 0.1944(1) | 0.1546(1) | 0.027(1) |
| In18 | 24d | 1 | 0.0706(1) | 0.2818(1) | 0.3553(1) | 0.023(1) |
| In19 | 24d | 1 | 0.1537(1) | 0.4571(1) | 0.3460(1) | 0.024(1) |
| In20 | 24d | 1 | 0.2379(1) | 0.2833(1) | 0.3563(1) | 0.024(1) |
| In21 | 24d | 1 | 0.0270(1) | 0.3596(1) | 0.2322(1) | 0.017(1) |
| In22 | 24d | 1 | 0.0278(1) | 0.3732(1) | 0.0805(1) | 0.021(1) |
| In23a | 24d | 0.77(5) | 0.1587(3) | 0.2823(2) | 0.4861(8) | 0.013(2) |
| In23b | 24d | 0.23(5) | 0.0090(30) | 0.1516(8) | 0.2125(11) | 0.018(6) |
| In24 | 24d | 1 | 0.0302(1) | 0.4783(1) | 0.1617(1) | 0.014(1) |
| In25 | 24d | 1 | 0.1537(1) | 0.1988(1) | 0.2738(1) | 0.026(1) |
| In26 | 24d | 1 | 0.1469(1) | 0.4085(1) | 0.1560(1) | 0.019(1) |
| In27 | 24d | 0.353(7) | 0.1569(2) | 0.2373(2) | 0.3664(2) | 0.019(2) |
| In28 | 8c | 0.54(2) | 0.0814(3) | *x* | *x* | 0.011(1) |
| In29 | 8c | 0.46(2) | 0.0998(4) | *x* | *x* | 0.023(3) |
| In30 | 8c | 0.56(2) | 0.0355(3) | *x* | *x* | 0.080(5) |
| Ca1 | 24d | 1 | 0.0361(2) | 0.3429(2) | 0.4669(2) | 0.014(1) |
| Ca2 | 24d | 1 | 0.2731(2) | 0.3486(2) | 0.4653(2) | 0.014(1) |
| Ca3 | 24d | 1 | 0.0396(2) | 0.1541(2) | 0.3425(2) | 0.010(1) |
| Ca4 | 24d | 1 | 0.1535(2) | 0.3394(2) | 0.2690(2) | 0.010(1) |
| Ca5 | 8c | 0.64(4) | 0.4636 | *x* | *x* | 0.019(3) |

$^a$ *U*(eq) is defined as one-third of the trace of the orthogonalized $U^{ij}$ tensor.

method. Down-folding techniques were automatically applied to the LMTOs, and scalar relativistic effects were included in the calculations. The band structure was sampled for 24 × 24 × 24 *k* points in the irreducible wedge of the Brillouin zone. Because of the computing limitations, only the electronic structure of 1/1 AC was calculated. To circumvent the disorder, the mixed and split positions were, for simplicity, considered as fully occupied by the predominant Au or In, and In8 was not considered. The handling of the disordered tetrahedron requires lowering the symmetry to *I*23 or *Pn*3. Since calculations in both subgroups resulted in negligible difference in total energies, *I*23 was chosen, as before.[15,17] These result in a unit cell content of "Ca$_{24}$Au$_{92}$In$_{52}$", which has a close composition and e/a value (1.76) to the experimental ones (e/a = 1.74).

## Results and Discussions

**Electronic Structure of Na$_2$Au$_6$In$_5$.** Figure 1 shows the densities-of-state (DOS) curves and the crystal orbital overlap population (COOP) data calculated (EHTB) for Na$_2$Au$_6$In$_5$. A

prominent feature is the pseudogap ($\sim$−6.5 eV) somewhat above the Fermi level ($E_F \approx$ −7.3 eV), together with empty Au−Au, Au−In and In−In states that are bonding at and above $E_F$ according to the COOP data, indicating that more electrons should better optimize the bonding. These effects are very similar to those previously found for the isotypic Mg$_2$Cu$_6$Ga$_5$.[16]

According to the calculations, $\sim$3.3 e$^-$/fu would be needed to push $E_F$ (e/a = 1.77) to the pseudogap (e/a $\approx$ 2.02) under a rigid band assumption. Since Na is too electropositive to mix (participate in covalent bonding) with the other elements, its replacement with another electron-richer "ICOSAGEN"[33] cation such as Mg, Ca, or Sc was considered useful. However, Ca is the better candidate (see below), considering both the apparent importance of low-lying d orbitals in the formation of Tsai-type QCs[15,34] and its size.[12] Thus, "Ca$_2$Au$_6$In$_5$" (e/a $\approx$ 1.92) was selected for the starting exploratory reaction.

**Syntheses and Phase Widths.** Figure 2a shows the product distributions among diverse compositions that were melted, slowly cooled, annealed, and analyzed by powder X-ray diffraction. Syntheses of compositions in the series CaAu$_x$In$_{6-x}$ (the horizontal row) were selected because the very first exploratory synthesis of the target "Ca$_2$Au$_6$In$_5$" luckily yielded mainly a phase isostructural with the recently reported Tsai-type 2/1 ACs Ca$_{13}$Cd$_{76}$[35] and Sc$_{11.17(2)}$Mg$_{3.04(2)}$Zn$_{73.54(2)}$.[17] This event suggested that the 1/1 AC and i-QC might also exist in this system and that the supposed 1/1 AC should crystallize in a YCd$_6$-type structure.[22] As can be seen, the main products successively changed from Ca$_4$Au$_{10}$In$_3$[36] to the 1/1 AC, the 2/1 AC, and AuIn$_2$ as x in CaAu$_x$In$_{6-x}$ varied as 4.5, 4, 3, and 2, corresponding to e/a values of 1.57, 1.71, 2.0, 2.29, respectively. In comparison, reactions with e/a fixed at 2.00 (vertical column) resulted in mainly variations from 2/1 AC to Ca$_2$Au$_3$In$_4$[37] as calcium proportions increased from 15% to 20%. In no case was the i-QC phase found under slow cooling and annealing conditions. Since e/a of the 2/1 AC ($\sim$2.03) is very close to the predicted values for the QC (2.02 from Na$_2$Au$_6$In$_5$, 2.00 from the 1/1 AC), the electronic search for the i-QC was narrowed to compositions in the range Ca:Au:In = (14−16):(40−44):(40−44), and the containers were directly quenched in water after melting. Remarkably, all these samples resulted in the formation of some i-QC (Figure 2b). The powder patterns of the 1/1 and 2/1 ACs and the i-QC are shown in black in Figure 2c together with the calculated powder patterns (red) for the ACs' according to single-crystal data. Note that these phases show larger peak widths compared with isostructural compounds. This is mostly likely related to the large absorption coefficient of Au on one hand and to the appropriate diffuse scattering (Figures S2 and S3) on the other, the latter probably arising from some structural disorder (discussed below).

Later on, the 2/1 AC samples were found to transform to i-QC after being remelted and quenched, whereas single-phase i-QC always transformed to 2/1 AC and AuIn$_2$ if remelted and slowly cooled to room temperature, indicating a spontaneous incongruent decomposition process. On the contrary, the 1/1

(33) King, R. B. *Inorg. Chem.* **1989**, *28*, 2796.
(34) Mizutani, U. In *The Science of Complex Alloy Phases*; Massalski, T. B., Turchi, P. E. A., Eds.; The Minerals, Metals & Materials Society: Warrendale, Pennsylvania 2005; pp 1−42.
(35) Pay Gómez, C.; Lidin, S. *Angew. Chem., Int. Ed.* **2001**, *40*, 4037.
(36) Lin, Q.; Corbett, J. D. Unpublished results.
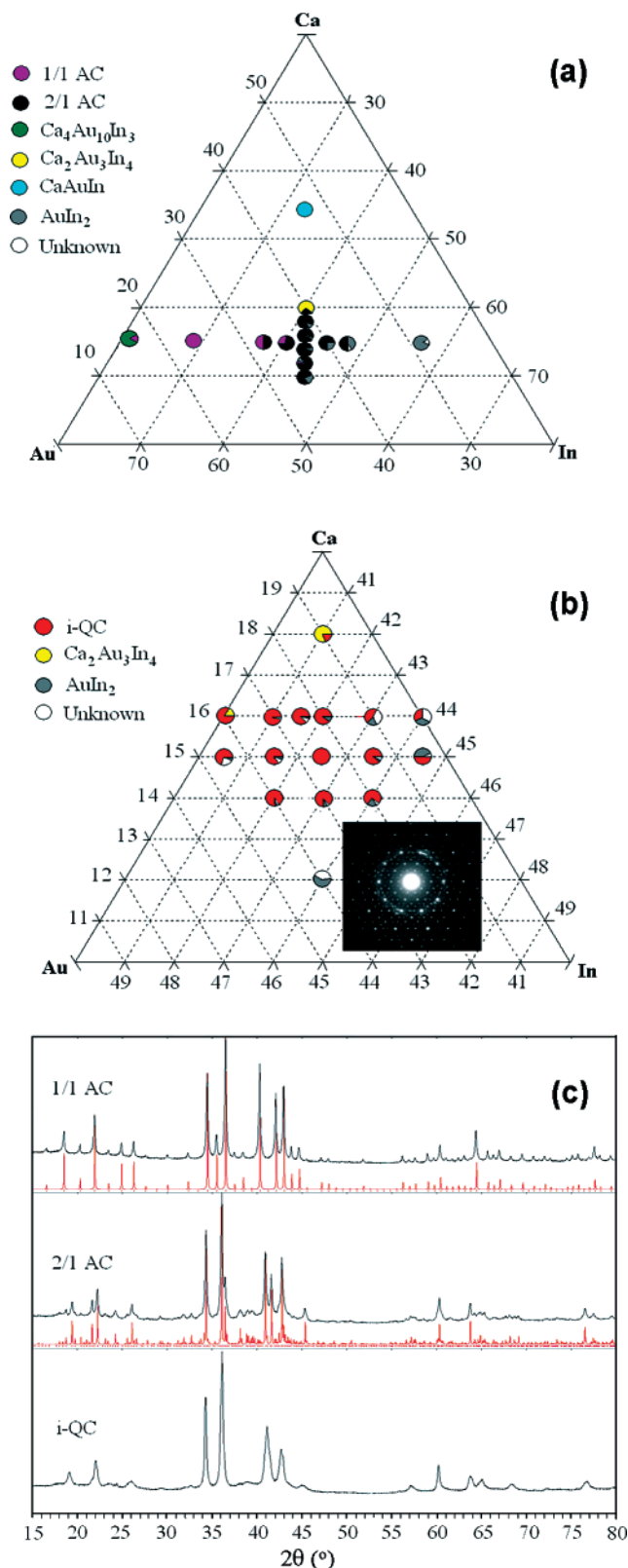(37) Hoffmann, R. D.; Pöttgen, R. *Z. Anorg. Allg. Chem.* **1998**, *625*, 994.

**Figure 2.** A portion of composition and phase analysis data for Ca−Au−In samples that were (a) slowly cooled from 850 °C and (b) quenched after melting at 850 °C. (Inset) ED pattern showing five-fold symmetry of i-QC. (c) Comparison of experimental (black) powder pattern data with those calculated (red) according to single-crystal data for ACs and i-QC (small vertical red bars are calculated peak positions). Note that the reflections show relatively lower intensities, greater peak widths, and somewhat diffuse scattering. (See also Figures S2 and S3.)
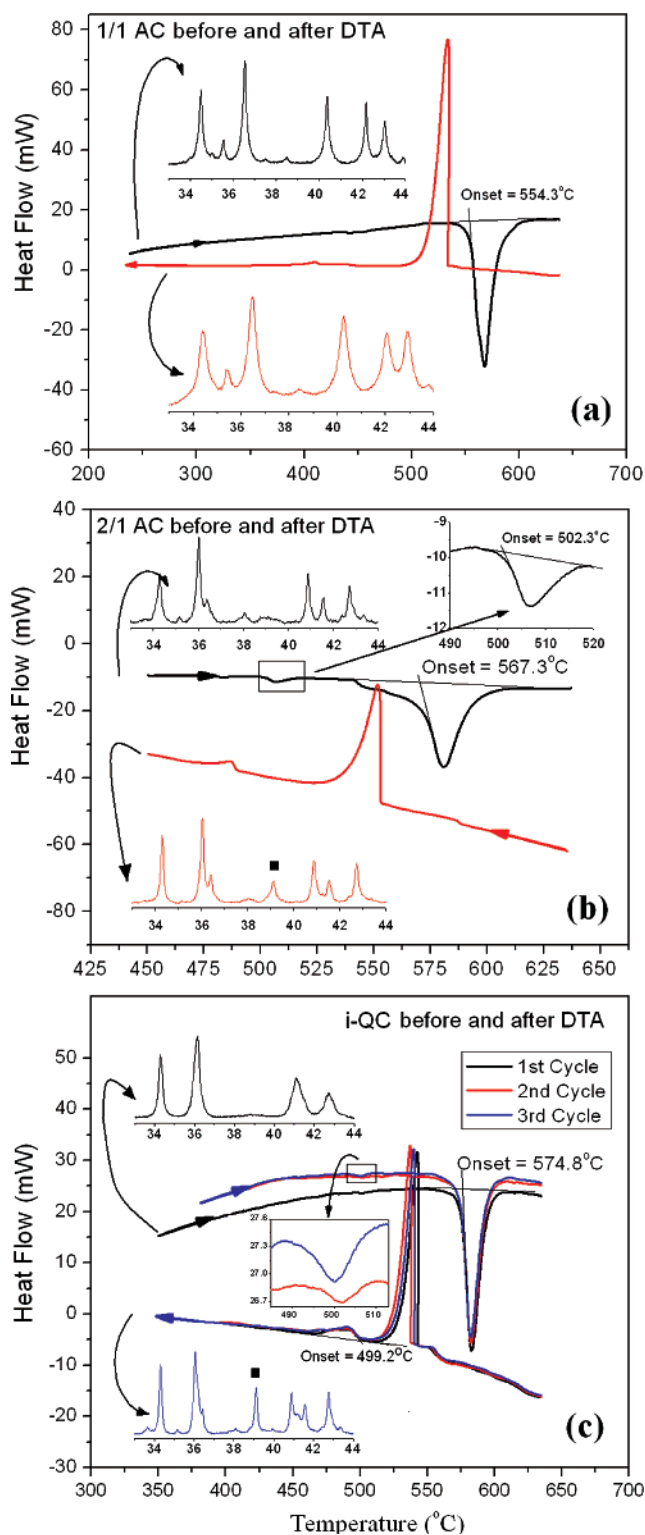


**Figure 3.** DTA data for (a) $Ca_3Au_{12.2(1)}In_{6.3(2)}$, 1/1 AC; (b) $Ca_{12.6(1)}Au_{37.0(2)}$-$In_{39.6(6)}$, 2/1 AC; and (3) $Ca_{14.1(2)}Au_{44.2(8)}In_{41.7(7)}$, i-QC. Black lines are on heating, and red lines, on cooling. Endothermal effects deflect downward. Insets show X-ray patterns before and after each run. Solid squares denote peaks from an $AuIn_2$ impurity.

AC remained unchanged on either quenching or slow cooling treatments. All these agree well with the DTA results (below).

Although no more efforts to determine accurate phase widths have been made, the AC lattice parameters (Table S3) refined from different samples varied within the ranges of 15.152(2)
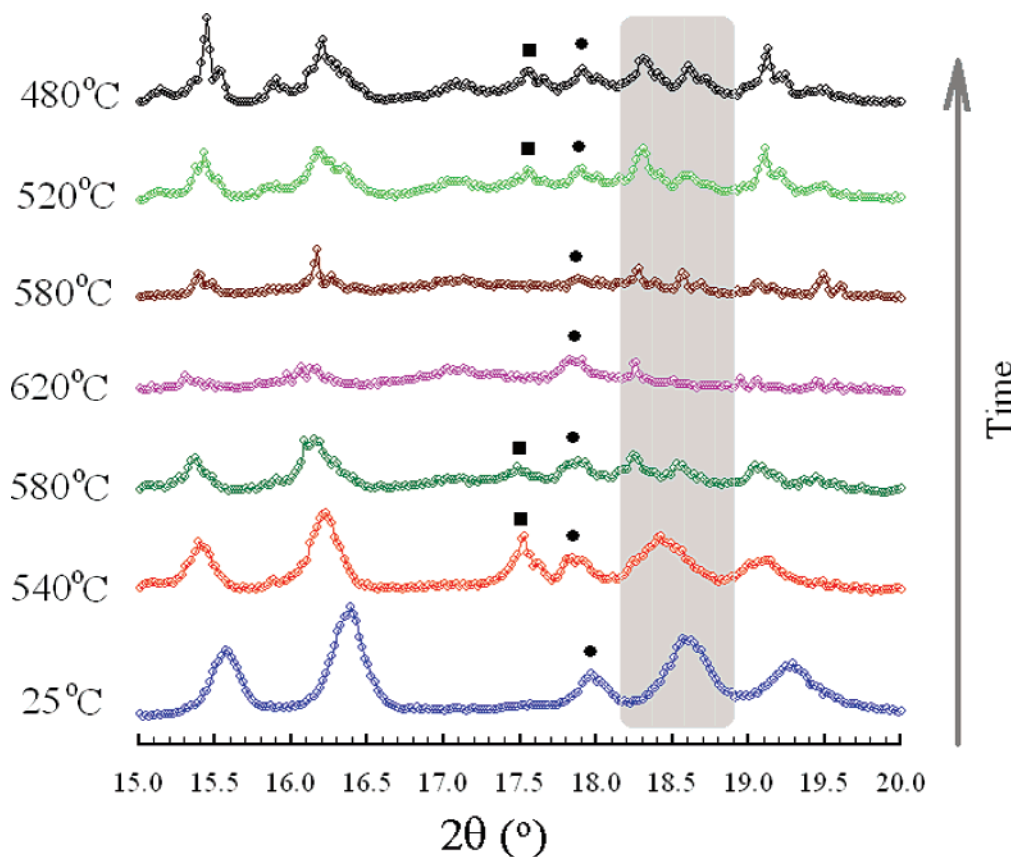
**Figure 4.** Selected temperature-dependent X-ray powder patterns (Mo Kα) for $Ca_{14.1(2)}Au_{44.2(8)}In_{41.7(7)}$ i-QC, showing in situ phase transitions as guided by the shaded region. Numbers mark temperatures at which patterns were recorded. Solid squares denote the reflection peaks from the $AuIn_2$ impurity. Solid circles denote those from the Pt sample holder.

± 0.012 Å and 24.632(3) ± 0.020 Å for 1/1 and 2/1 ACs, respectively, and the respective compositions varied within ∼2.3 atom % and ∼2.7 atom % in terms of relative refined Au/In proportions. The lattice constant of the i-QC refined from six strongest reflections using Elser's method[38] only varied over 5.538(3) ± 0.003 Å. These data all suggest narrow phase ranges, paralleling the Au/In mixing in both ACs and i-QC, and consistent with the experimental results shown in Figure 2a and 2b.

**Phase Stabilities.** Panels a–c of Figure 3 show the DTA data for 1/1 AC, 2/1 AC and i-QC samples, respectively, together with the Guinier powder patterns of each before and after scanning. As can be seen, the 1/1 AC exhibits only fusion/solidification changes during DTA measurements (Figure 3a), indicating a stable phase under these conditions. The heating and cooling curves of the 2/1 AC in Figure 3b show two reversible changes (∼502 °C and ∼567 °C on heating). The latter corresponds to the fusion/solidification of the 2/1 AC, whereas the former is also observed in i-QC cooling process (below). Powder patterns before and after the cycle indicates that the 2/1 AC phase remains. (The diffraction peak at about 39.2° is from $AuIn_2$ impurity, which results in a pre-tail below the endothermic melting peak at ∼540.7 °C.[39]) In order to track the endothermic event at ∼502 °C, one heated 2/1 AC sample was quenched at 530 °C. Surprisingly, the powder pattern showed that the 2/1 AC phase remained unchanged, but with

more $AuIn_2$. The same results were also observed in in situ temperature-dependent phase analyses (Figure S4). These may imply the effect is simply not quenchable under these conditions.

The DTA data of i-QC sample suggest a complicated process. Upon heating, no obvious endothermic transition can be observed until melting (∼575 °C); however, a small exothermic peak appears at about 500 °C on slow cooling. Phase analyses at this stage reveal that i-QC had transformed to 2/1 AC plus $AuIn_2$. Therefore, two more heating–cooling cycles were performed and powder patterns recorded after each cycle. The thermogram and XRD pattern thereafter (Figure 3c) are very similar to that in Figure 3b. Note that the intensity of the reflection at ∼39° increases, suggesting that the $AuIn_2$ phase accumulates as reaction continues, perhaps because the QC decomposition is somewhat incongruent. Although the exothermic solidification peaks shift somewhat (possibly related to the appreciable compositional variation mentioned above), the peaks at ∼500 °C always overlap. In the other side, independent annealing of the i-QC at 530 °C for 1 month induces phase transformation to 2/1 AC, whereas at 450 °C for one week produces no phase change. All of these facts suggest that the peak at ∼500 °C represents the transformation between i-QC and stable 2/1 AC phases, and that the states giving this peak are very similar in structure, as suggested by the small heat effect involved in this peak, ∼3.0 J/g. The temperature-dependent XRD patterns of i-QC shown in Figure 4 reveal that the i-QC phase on heating appears to transform to 2/1 AC and $AuIn_2$ around its melting point. Above the melting/decomposi-

(38) Elser, V. *Phys. Rev. B* **1985**, *32*, 4892.
(39) Storm, A. R.; Wernick, J. H.; Jataraman, A. *J. Phys. Chem. Solids* **1966**, *27*, 1227.
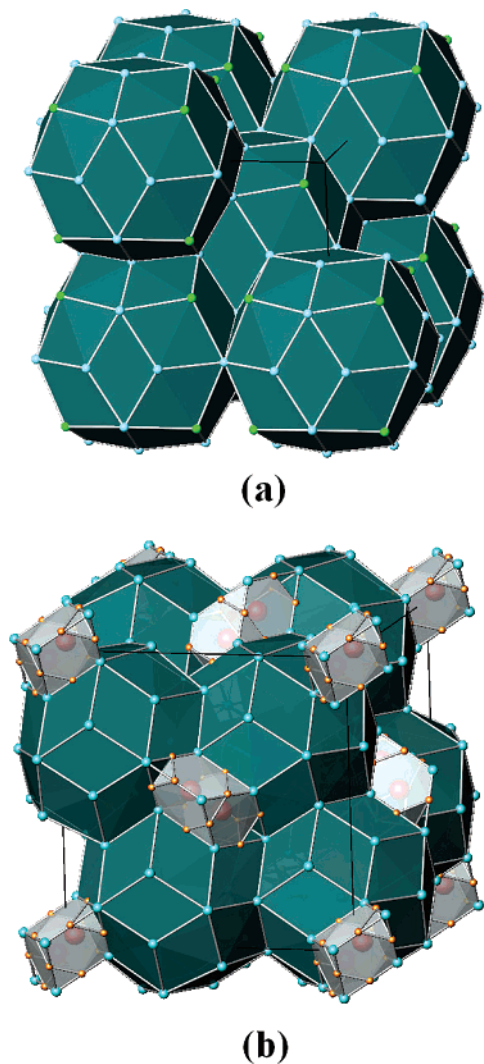
**(a)**

**(b)**

**Figure 5.** Unit cell representations of (a) $Ca_3Au_{12.2(1)}In_{6.3(2)}$ 1/1 AC, with bcc packing and (b) $Ca_{12.6(1)}Au_{37.0(2)}In_{39.6(6)}$ 2/1 AC, primitive cubic, each with the packing of interpenetrating triacontahedral clusters. For clarity, decoration atoms at or near the centers of triacontahderal edges are omitted, and one triacontahedron in the 1/1 AC cell is omitted in order to see the bcc packing. Note that the spaces left in (b) after the triacontahedral clusters are condensed generate prolate rhombohedra (PR). Each PR holds a double Friauf polyhedra (gray) which is centered by a Ca–Ca dimer. (Green) Au/In. (Blue) In. (Red) Ca. (Golden) Au. The same scheme applies to Figure 6.

tion point, the diffraction peaks of 2/1 AC appear with low intensities and larger peak widths, possibly related to a peritectic melting process. The cooling results are the same as those observed for 2/1 AC (Figure S2), consistent with the DTA results.

**Structural Descriptions.** As found before for the Sc–Mg–Zn and Al–Mg–Zn 2/1 ACs,[40,41] the unit cell contents of the present Tsai-type 1/1 and 2/1 ACs are also well represented by body-centered cubic and primitive cubic packing of triacontahedral clusters (Figure 5). Each of these encapsulates a so-called Tsai-cluster made up of four endohedral shells; from center out, a disordered tetrahedron, a dodecahedron, an icosahedron, and an icosidodecahedron (Figure 6). Since the cluster geometries and linkages for both long-range periodic order and short-range
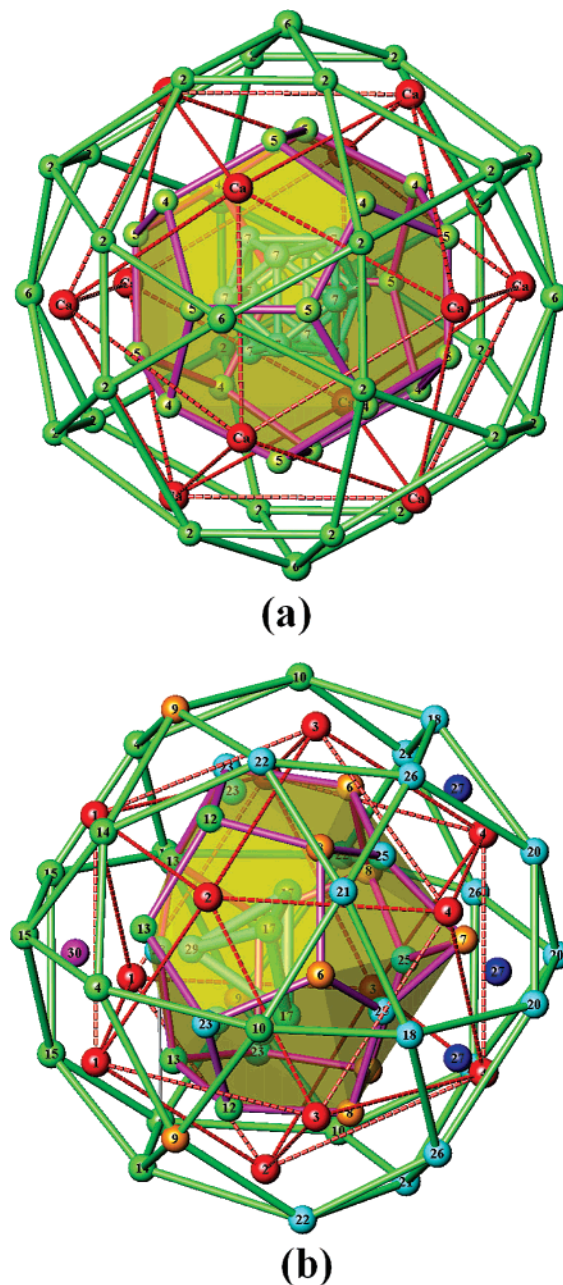
(40) Lin, Q.; Corbett, J. D. *J. Am. Chem. Soc.* **2006**, *128*, 13268.
(41) Lin, Q.; Corbett, J. D. *Proc. Natl. Acad. Sci. U.S.A.* **2006**, *103*, 13589.

**(a)**



**(b)**

**Figure 6.** Comparison of multi-endohedral Tsai-clusters within triacontahedral clusters in (a) 1/1 and (b) 2/1 ACs. Atom legends are the same as for Figure 5, except for the additional fractional In27 (blue) and In30 (purple) atoms.

order are very similar to those in Sc–Mg–Zn ACs,[40] the only difference here being the greater structural disorder (including both occupancy and positional disorder), we will focus on the disorder problems rather than reiterate the similarities described in refs 40 and 41.

The shell contents of both ACs are enumerated in Table 3 together with those of the corresponding Sc–Mg–Zn ACs.[40] As can be seen, the constitutions of the dodecahedral, icosidodecahedral, and triacontahedral shells for the two current ACs are quite different from each other, in contrast to the similarities for those pairs in the Sc–Mg–Zn ACs. Both the second and the fourth shells have notably higher In proportions in the 2/1 AC, whereas the important triacontahedron becomes pure In. As a result, the overall e/a values for 1/1 and 2/1 differ

**Table 3.** Comparison of Shell Contents within Triacontahedra in Tsai-Type 1/1 and 2/1 ACs in the Ca−Au−In and Sc−Mg−Zn Systems[40]

| | Ca−Au−In (ACs) | | Sc−Mg−Zn (ACs) | |
| --- | --- | --- | --- | --- |
| polyhedron | 1/1 | 2/1 | 1/1 | 2/1 |
| tetrahedron[a] | $In_4$ | $In_{3.5}$ | $Zn_4$ | $Zn_{2.9}$ |
| dodecahedron | $Au_{15.3}In_{4.7}$ | $Au_{10.2}In_{9.3}$ | $Zn_{20}$ | $Zn_{19.4}$ |
| icosahedron | $Ca_{12}$ | $Ca_{12}$ | $Sc_{12}$ | $Sc_{9.6}Mg_{2.4}$ |
| icosidodecahedron | $Au_{20.7}In_{9.3}$ | $Au_{11.0}In_{19.0}[In_{1.6}]$ [b] | $Zn_{29.2}Mg_{0.8}$ | $Zn_{29.3}Mg_{0.7}$ |
| triacontahedron[c] | $Au_{6.8}In_{25.2}$ | $In_{29.6}$ | $Zn_{32}$ | $Zn_{32}$ |
| | $(Au_{54.0}In_{6.0})[In_{3.8}]$[c] | $(Au_{48.0}In_{12.0})$ | $(Zn_{60})$ | $(Zn_{60})$ |
| e/a | 1.73 | 2.03 | 2.14 | 2.13 |

[a] Disordered tetrahedron in 1/1 and fractional tetrahedron in 2/1 AC. [b] Contents in square brackets are fractional atoms located between shells. [c] Contents in parentheses are additional decorations at or near the center of the edges of the triacontahedral clusters.
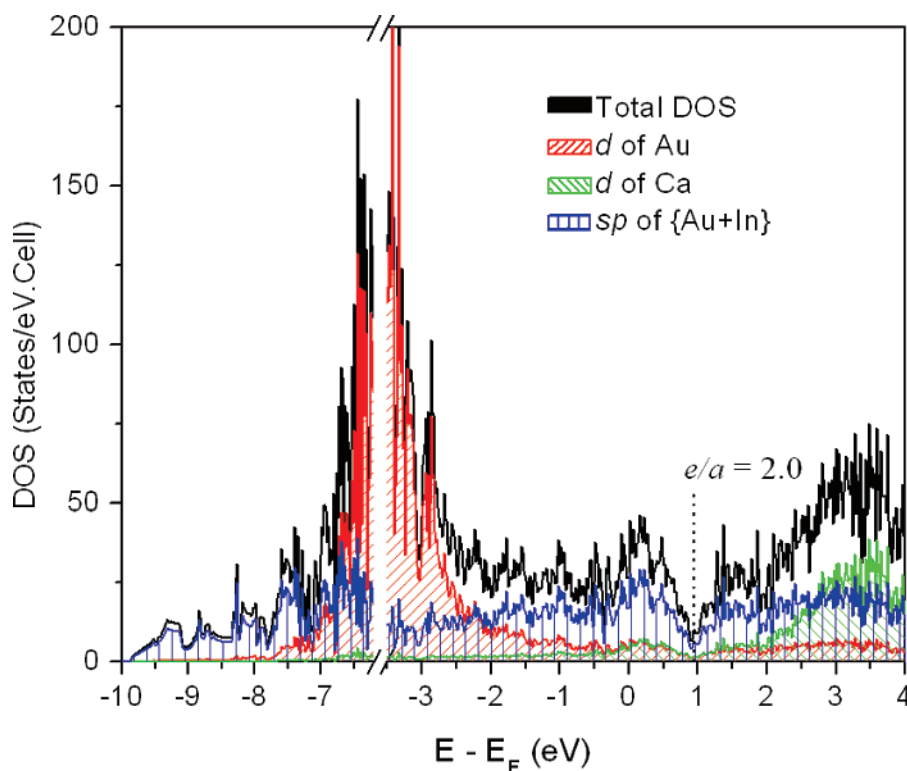


**Figure 7.** DOS of the $Ca_{24}Au_{92}In_{52}$ 1/1 AC model calculated by ab initio methods. The i-QC was subsequently synthesized from a composition at the pseudogap (e/a ≈ 2.00).

considerably (1.73 vs 2.03). Actually, this appears to be the first case in which the 1/1 and 2/1 AC structures have such large differences in shell contents and e/a values. The reason may relate to the much more similar Au vs In metallic radii (CN = 12, Au: 1.439; In: 1.579 Å) than for Mg vs Zn (CN = 12, Mg: 1.598; Zn: 1.339 Å).[42] The former are presumably less discriminating and afford more atomic mixing and substitution while retaining the same structure types. This must also show up in energy terms, which enable s, p, d orbital mixings up to $E_F$ (below).

The positional disorder in the 1/1 and 2/1 ACs are remarkable. The YCd$_6$-type 1/1 ACs commonly show very anisotropic atomic displacements parameters (ADP) for atoms on the innermost tetrahedra, but that is not the case here. The Ca−Au−In 1/1 AC shows rather isotropic ADPs for atoms in the tetrahedral shell; instead, positional disorder occurs in the dodecahedral shell (Tables 2 and S1). The same holds for the 2/1 AC. Positional disorder is commonly found in other ACs

(e.g., $Al_{57.3}Cu_{31.3}Ru_{11.3}$,[43] $Al_{66.5}Rh_{26.1}Si_{7.3}$,[44] $Ca_{13}Cd_{76}$,[35] $Yb_{13.2}$-$Cd_{76.1}$[45]) and many other intermetallics. In essence, this may generally reflect generally lower differentiation both radially (size) and chemically. Actually, the positional disorder (dephasing) may be the reason why the powder patterns show larger peak widths and diffuse scattering (Figures 2, 3, S2, S3). Numerous larger residual peaks (Table 1) in the final difference Fourier map also suggest high background noise from diffuse scattering that is presumably generated by this (and other) disorder. Note that we tried to grow crystals with less positional disorder by optimizing element proportions and reaction conditions, but these defects do not disappear even after annealing at 500 °C for 1 month. We have not yet pursued more quantitative measures of the relative amounts of diffuse scattering for these phases.

(42) Pauling, L. *The Nature of the Chemical Bond*, 3rd ed.; Cornell University Press: Ithaca 1960; pp 393−448.

(43) Sugiyama, K.; Kato, T.; Ogawa, T.; Hiraga, K.; Saito, K. *J. Alloy Compd.* **2000**, *299*, 169.
(44) Sugiyama, K.; Sun, W.; Hiraga, K. *J. Non-Cryst. Solids* **2004**, *334* and *335*, 156.
(45) Pay Gómez, C. *Order and Disorder in the RE-Cd and related systems*; Stockholm University: Sweden, 2003.

The positional disorder actually appears to play important roles in structural stabilization. Figure 6b shows the multi-endohedral shells within a triacontahedron in the 2/1 AC and the pertaining disordered atoms. As can be seen, the innermost tetrahedron (blue) is again not at the common center of the outer polyhedra but shifted along the 3-fold axis, leaving space to the right of the triangle base (Au/In17 atoms). The same geometry is observed in Sc−Mg−Zn 2/1 AC,[40] but not in the Ca$_{13}$Cd$_{76}$[31] or Yb$_{13}$Cd$_{76}$ 2/1 ACs[35,45] which both contain many split positions inside the dodecahedron. However, In27 (blue) sites, new in the 2/1 AC array, are observed outside of the dodecahedron in the present case. Note that there are also three other equivalent In27 (not shown) beyond the icosidodecahedron, being vertices of the outmost triacontahedral shell. The appearance of these sites is associated with distortion of the dodecahedron (on the blue atom side) and positional splitting (In23) which both appear to relieve bonding stress.

**Electronic Structure of 1/1 AC.** Figure 7 shows the DOS calculated by ab initio means for the 1/1 AC. As can be seen, the broadened d orbitals of Au are mainly populated over about a −7 to −2 eV energy range, whereas the s, p orbitals of Au plus In and the d orbitals of Ca are widely spread over the whole band. (Although DOS for Ca d and Au d appear comparable at $E_F$, the Ca effect is notably greater at that point because the number of atoms in the formula (or cell) is as 1:4.) The s, p orbitals of Ca also spread over the whole energy range, but their projected DOS are low everywhere (<6 states/eV·cell, not shown).

A prominent feature of the 1/1 AC DOS curve is that a pseudogap exists at e/a = 2.00, close to both values predicted (2.02) from EHTB on Na$_2$Au$_6$In$_5$ and that experimentally discovered (1.98) for the i-QC. Judging from the projected DOS curves, Au, In s and p, and Ca d orbital mixing make major contributions to the formation and deepening of the pseudogap (hence, to the i-QCs), similar to the effects noted in the Sc−Mg−Zn[17] and Sc−Mg−Cu−Ga systems.[15] This conversely supports the choice of Ca, not Mg, in our experimental design. Calcium not only offers more valence electrons than the original Na, so that the $E_F$ is driven toward the pseudogap, but it also provides the d orbitals that help the formation or deepening of pseudogap according to Muzutani.[34] (A parallel calculation with Mg on the Ca position reveals no pseudogap around $E_F$.) These results appear to convey significant amounts of information about the electronics in other interesting phases. In fact, further studies in which Ca has been replaced by Yb, with lower-lying d orbitals and a similar size, again reveal 1/1, 2/1 ACs and i-QC phases.[36] Meanwhile, attempts to use Mg or Sc to achieve the same goal in the M−Au−In systems result in unexpected phases.

## Conclusions

The work presents another example of tuning to the 1/1 and 2/1 ACs and to the i-QC, here in the Ca−Au−In ternary system, utilizing the recently proposed pseudogap prediction method.[15] The 1/1 AC, Ca$_3$Au$_{12.2(1)}$In$_{6.3(2)}$, crystallizes in the space group $Im\bar{3}$, whereas the 2/1 AC, Ca$_{12.6(1)}$Au$_{37.0(2)}$In$_{39.6(6)}$, in the space group $Pa\bar{3}$, the same pair as found earlier in both the Sc−Mg−Cu−Ga[15] and Sc−Mg−Zn[40] systems. Structure analyses reveal that both AC compounds again have triacontahedral clusters as their basic building blocks at the unit cell level and similar short-range-ordered Tsai-type structural motifs within, but with major difference in the long-range order of the triacontahedra, as before.[40,41] Appreciable positional disorder is found in the present ACs in comparison to earlier isostructural examples.

DOS analyses of the 1/1 AC reveal the presence of a pseudogap at e/a = 2.00, at which point the i-QC indeed exists, consistent with the predictions from band structure analyses of Na$_2$Au$_6$In$_5$ as well, even though these compounds exhibit three different structure types. The sp−d orbital mixing around the Fermi energy appears to play important roles in the formation and deepening of pseudogap. DTA, and phase analyses suggest that 1/1 and 2/1 ACs are stable up to their respective melting points, whereas the i-QC is metastable below ∼500 °C.

JA069143X